Improvements in epitaxial lateral overgrowth of InP by MOVPE

Nick H. Julian *, Phil A. Mages, Chong Zhang, John E. Bowers

Department of ECE, Engineering Science Building, Room 2221C, University of California, Santa Barbara, CA 93106, USA

ARTICLE INFO

ABSTRACT

Indium phosphide and silicon play important and complementary roles in communications wavelength photonic devices. Realizing high quality coalesced epitaxial lateral overgrown (ELO) InP films on Si could greatly reduce cost and encourage the proliferation of energy efficient photonic integrated circuits in consumer devices. By adjusting a parallel line ELO mask and metalorganic vapor phase epitaxial growth conditions, we have fully coalesced and partially coalesced epitaxial lateral overgrowth of InP on InP substrates and Si substrates having strain relaxed III/V buffer layers, respectively. Extended defects were investigated using transmission electron microscopy and were not found to originate at the coalescence of the nearest neighbor growth fronts for linear parallel growth windows oriented 60° off of $[0-11]$ when using a high V/III ratio of 406. In addition, narrowly separated linear parallel growth windows having a large aspect ratio of 7.5 were seen to inhibit the upward propagation of stacking faults through several neighboring openings. Elimination of these two defect sources would leave primarily the challenge of optimizing the morphology of the overgrown InP as a substantial barrier to achieving coalesced ELO InP of sufficient quality for photonic device applications.

1. Introduction

An epitaxial method for realizing high quality InP films on a Si substrate is currently desirable for enhancing functionality and lowering cost of electronic and photonic devices. Bonding of InP to Si wafers has been very successful for creating lasers and other active devices [1], but InP substrate cost and complications in scaling to larger wafers (> 150 mm) used in the Si electronics industry highlight the need for an epitaxial alternative. Unfortunately, due to the large thermal and lattice mismatch of InP to Si, 77% and 8% respectively, direct heteroepitaxial growth results in prohibitively high densities of extended defects ($\sim 10^9 \, cm^{-2}$) which provide paths for non-radiative recombination as well as proliferation of dark line defects (DLD) and dark spot defects (DSD) [2]. Epitaxial lateral overgrowth (ELO) is one promising method for inhibiting the presence of extended defects in appropriately large regions of device material [3].

The ELO method begins with a selective area growth (SAG) using an amorphous material as a growth inhibiting mask layer. Openings are patterned into this layer to allow growth to initiate on the substrate below and propagate upward. Once growth has crested above this mask it is then free to propagate laterally and eventually coalesce with neighboring growths, if its morphological behavior encourages such lateral growth.

The primary advantage of the ELO process is the proven ability to terminate dislocations propagating from the lower layer onto the patterned amorphous layer during the selective area growth step [4]. The primary challenges faced by ELO are the prevention of defect formation during coalescence, the inhibition of planar defects from propagating through the mask openings to the upper surface, and the optimization of growth morphology to increase lateral growth rates and overgrowth uniformity. This paper addresses each of these issues.

Preventing the propagation of planar defects such as stacking faults (SFs) and anti-phase boundaries (APBs) is difficult due to their two dimensional geometry, which may extend along the length of a linear mask opening as growth proceeds upward. Fig. 1a illustrates the typical defect diversity found in InP grown directly on Si (100) substrates miscut 4–6° toward [111]. As is seen, planar defects have a significant presence in heteroepitaxial InP on Si. Among these, an abundance of intrinsic Shockley type faults may be attributed to the low stacking fault energy of InP which provides an insufficient energy barrier to inhibit dissociation of a dislocation into two Shockley partial dislocations separated by an intrinsic stacking fault under the influence of stress induced by lattice and thermal mismatches [5]. Fig. 1b illustrates the possible planar defect geometry and propagation through a linear ELO mask opening. If the planar defect is a stacking fault, then its propagation through the mask window is determined by the behavior of the partial dislocations which bound it within the ELO mask window [6].

* Corresponding author. Tel.: +1 805 893 2149; fax: +1 805 893 7990.
E-mail address: njulian@engr.ucsb.edu (N.H. Julian).

Favorable inhibition of planar defects has been demonstrated by carefully engineering the III–V/IV interface within shallow trench isolation (STI) structures and by selecting a particular SAG line direction [7]. Unfortunately the volume of useful material within these SAG regions is too small and in too close proximity to a reservoir of dislocations that may expand to produce dark line defects (DLD) during laser operation. Upward diffusion of group IV elements has also been noted by Merckling et. al. [8]. Lateral overgrowth makes a larger volume of active material available for device formation, with potentially greater isolation from propagating defects and diffusing species. Growth through STI trenches at the angles used to minimize planar defects has yet to demonstrate favorable lateral overgrowth and coalescence quality.

In this work, we demonstrate a dependence of coalescence induced dislocations on ELO parallel stripe orientation for indium phosphide grown by metal-organic vapor phase epitaxy (MOVPE) with a V/III ratio of 406. Transmission electron microscopy (TEM) is used to examine both homoepitaxial ELO on InP substrates and heteroepitaxial ELO on Si substrates having strain relaxed III/V buffer layers. We use the morphological control enabled by MOVPE to obtain favorable results in which none of the defects detected in the coalesced layer are attributable to coalescence alone, but appear in
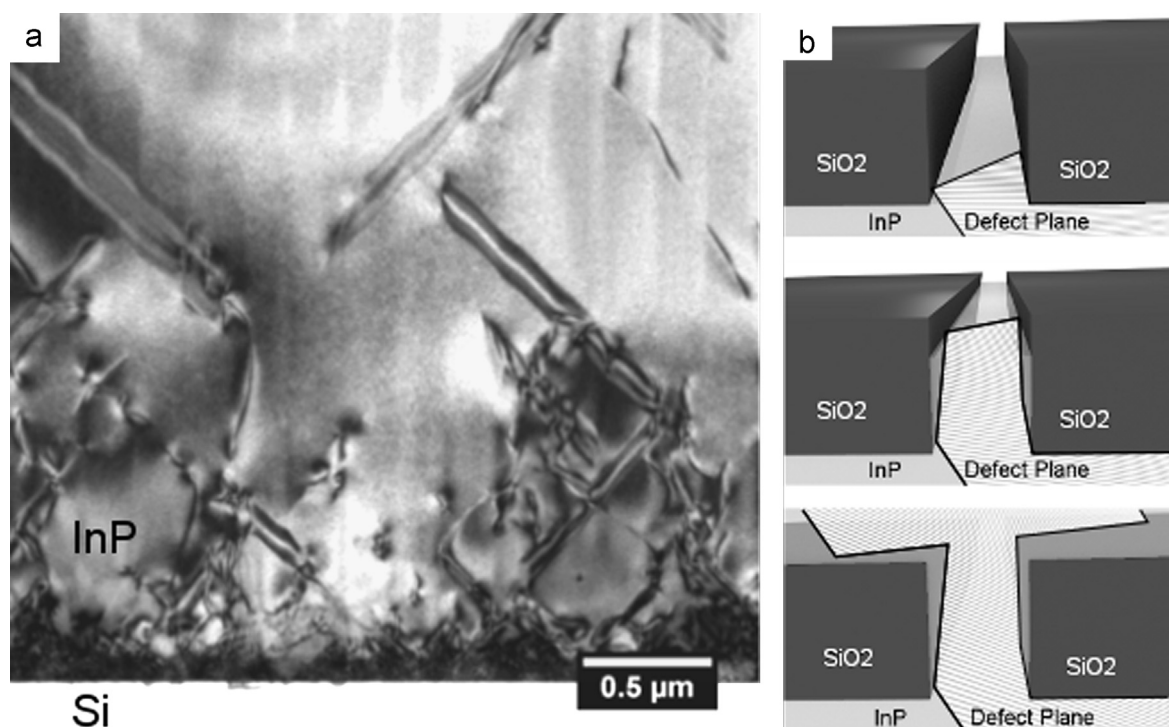
Fig. 1. (a) Cross-sectional TEM of InP grown on miscut (100) Si substrates showing planar defect prominence. (b) Illustration of worst-case planar defect growth through linear SAG mask and expansion into upper ELO material.

Table 1
List of ELO growths and mask patterns explored. Each growth series listed represents a single MOVPE growth in which multiple patterns were included. Angles refer to orientations of linear openings rotated away from [0–11] about [100]. Clockwise and counter-clockwise rotations of linear openings away from [0–11] are equivalent by crystal symmetry.

Growth series	Mask thickness (nm)	Opening width	Separation between openings	Mask pattern (deg)	Figure
Micrometer scale homoepitaxy	200	0.8 μm	5 μm	Linear 30	2(e,f,g,h),3(c)
				Linear 60	2(a,b,c,d),3(a,b)
Holographic homoepitaxy	200	100 nm	110 nm	Linear 60	6(a)
Micrometer scale heteroepitaxy w/MQW	200	0.8 μm	1 μm	Linear 60	5(c)
		0.8 μm	2 μm		
		0.8 μm	5 μm	Linear 0	5(a)
				Linear 30	4(b), 5(a)
				Linear 60	4(a), 5(a,b,c)
				Linear 90	5(a)
				Disk	5(a)
		1 μm	5 μm	Linear 60	5(a,b)
		1.2 μm	5 μm		
		2 μm	5 μm		
		5 μm	5 μm		
		10 μm	10 μm		
Emergent holographic heteroepitaxy	750	100 nm	110 nm	Linear 60	6(b)
Coalesced holographic heteroepitaxy	750	100 nm	110 nm	Linear 60	6(c), 7, 8,9
Polished holographic heteroepitaxy	500	100 nm	110 nm	Linear 60	6(d)

conjunction with other defect sources including poor morphology, planar defects, and dry etch redeposition. We also note several instances in which stacking faults fail to reach the uppermost ELO region, as well as an intermittent elimination of stacking faults when propagating through closely pitched high aspect ratio linear ELO windows.

2. Experimental procedure

Each ELO mask was created using a chromium hard-mask process to minimize polymeric contaminants created during dry etching. A desired SiO_2 thickness, ranging between 200 nm and 750 nm, was first deposited by inductively coupled plasma
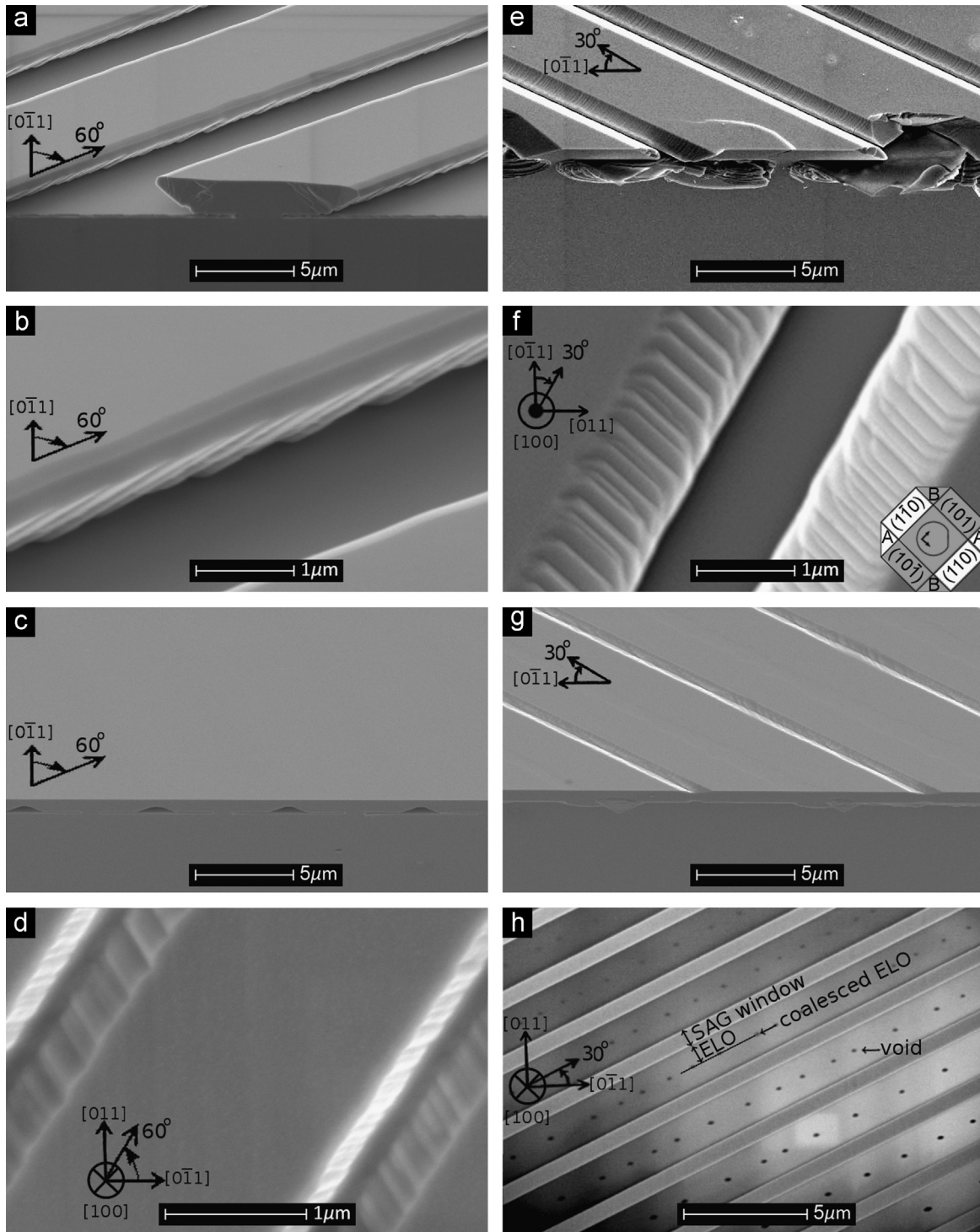

Fig. 2. Scanning electron microscope (SEM) images illustrating the sequence of coalescence for the two primary growth profile variations, dependent on stripe direction. (a–c) show a tilted perspective of the cross-sectional profile of growth through lines 60° off of [0–11], and the resulting smooth upper coalesced surface. Steps of facets are seen on the underside of these coalesced ledges when the substrate is milled away by focused ion beam in (d). (e–g) show the profile and upper surface of growth through lines 30° off of [0–11] with upward facing faceted steps which resulted in voids from two-zipper coalescence that are revealed when viewed from the underside in (h). Inset to (f) is a projected rhombicuboctahedron illustrating the positions of {111}A, (110), and (1−10) planes which bound the faceted steps. Coalescence of homoepitaxial lines with 5 μm separation shown in (c,d,g,h) required only a nominal growth thickness of 1.2 μm. The [0−11] coordinate axis and SAG window angle are drawn projected within the tilted (100) plane of the upper surface for (a–c,e,g).

enhanced chemical vapor deposition at 250 °C. Cr was then deposited onto the sample by electron beam evaporation. We then used one of two lithographic techniques to define the pattern to be etched into the Cr layer. To achieve feature sizes of 0.8 μm and larger, we used conventional i-line lithography to define a pattern in photoresist. To achieve smaller features, a holographic setup using a single mirror and a 325 nm He–Cd laser was used to define 210 nm pitched parallel lines with 110 nm openings in photoresist on top of an XHRiC-11 antireflective coating (ARC). The 210 nm pitched lines with 110 nm openings were subsequently etched into the antireflective coating using an O_2 plasma at 150 mTorr. Following either lithography process, the pattern was etched into Cr using a Cl_2+O_2 inductively coupled plasma (ICP) etching. The holographically defined samples then had any remaining ARC removed with an O_2 plasma, and the underlying SiO_2 etched via ICP. The Cr hard-mask was removed from all samples with the same Cl_2+O_2 etch as above. The surface was treated with sulfuric acid immediately prior to growth.

Growth was carried out in a Thomas Swan horizontal MOVPE reactor with 5 cm susceptor, using tertiary butyl phosphine (TBP) and trimethylindium (TMI) as precursors in a hydrogen carrier gas. A high V/III ratio of 406 was used with nominal growth rates between 0.2 nm/s and 0.4 nm/s at 615 °C and 350 Torr, as suggested by a prior work to achieve optimal morphology and lateral growth of homoepitaxial ELO lines 60° off [0 − 11] [9,10]. In this work we use the coordinate system having [100] normal to the upper surface of the wafer, and [111] normal to a (111)A plane.

A homoepitaxial approach was first used to determine if a favorably low density of coalescence related defects could be achieved without the complications introduced by heteroepitaxy. For this, parallel lines oriented 60° and 30° away from [0 − 11], and having 0.8 μm wide openings with varying separations were patterned into 200 nm thick SiO_2 on (100) InP substrates.

Heteroepitaxial ELO coalescence was studied using an InP seed layer grown by IQE plc on a graded metamorphic buffer of $In_xAl_{1-x}As$, which was itself grown on a GaAs buffer layer upon
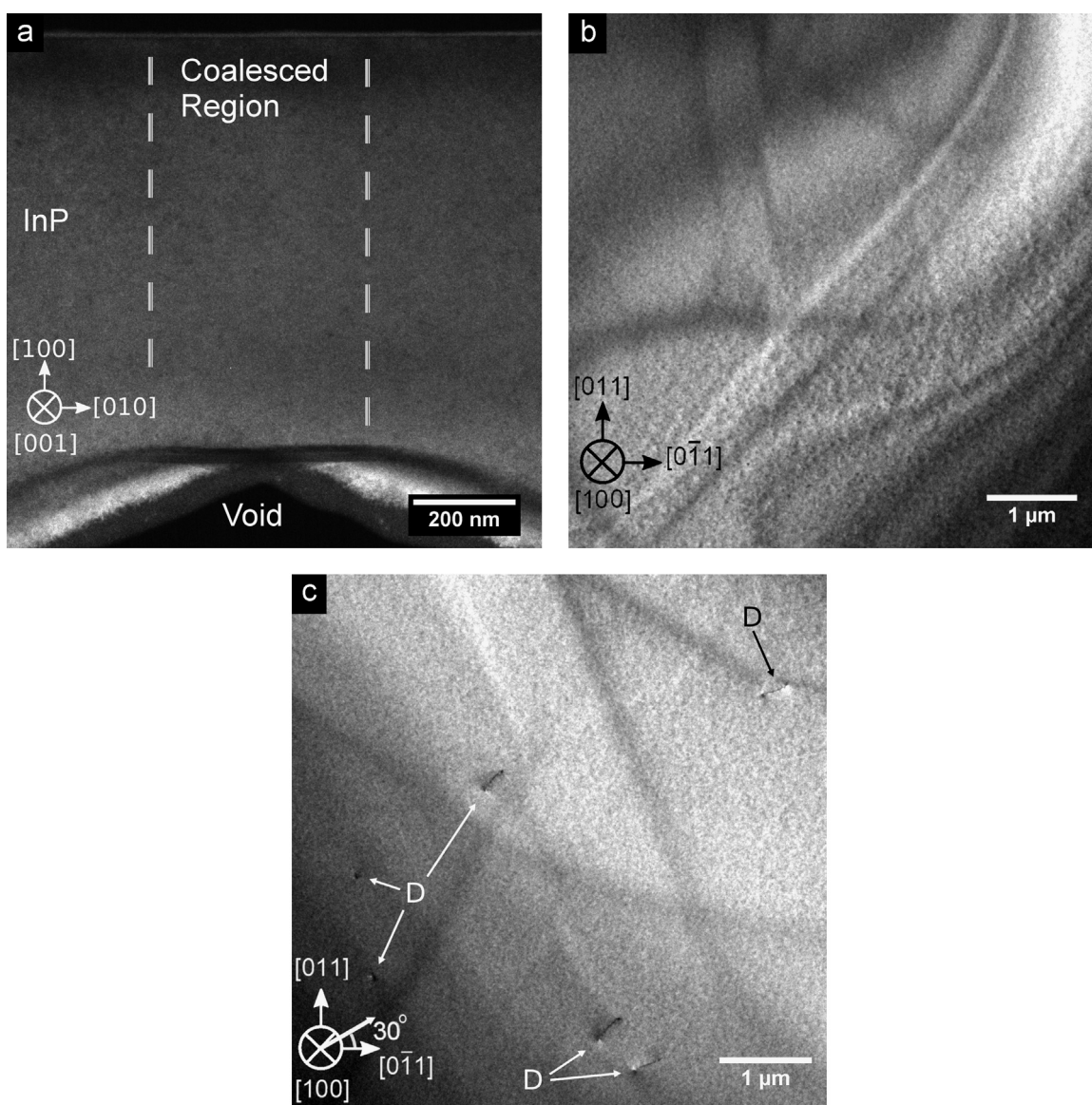
Fig. 3. (a) Cross-sectional dark field TEM of coalesced region for homoepitaxial ELO using lines 60° off of [0 − 11] showing no coalescence generated defects. (b) Plan view TEM of fully coalesced homoepitaxial ELO film using lines 60° off of [0 − 11], showing a complete absence of extended defects. The continuous curves shown in these low magnification plan view images are due to variations in sample thickness and bending, and are not crystallographic defects. (c) Plan view TEM of fully coalesced homoepitaxial ELO film using lines 30° off of [0 − 11] showing dislocations labeled "D". The rough texture seen in plan view is attributable to lamella surface roughness and contamination from the FIB/SEM preparation method. The ⟨400⟩ family of g vectors was used to construct the diffraction conditions for these images.

a miscut (100) silicon substrate [11,12]. The total thickness between silicon substrate and the top of the InP seed layer was approximately 2.7 μm. The same patterns applied to the homo-epitaxial samples were applied here, except we increased the SiO₂ thickness to 500 nm and 750 nm for the holographically defined nano-lines to explore the possible effects of higher aspect ratio masks on planar defect propagation, the existence of which are suggested by the results of Wang et al., [7]. Table 1 lists all growth series and corresponding mask patterns included in this paper.

Resultant growths were examined via scanning electron microscopy (SEM) and cross-sectional transmission electron microscopy (TEM). TEM lamellae were prepared by focused ion beam (FIB) in-situ a scanning electron microscope.

3. Results and discussion

3.1. Homoepitaxial coalescence of micrometer scale parallel lines

MOVPE ELO growth shape and morphology have previously been shown to correlate with extended defect formation at coalescent regions between growth fronts separated by narrow angles [9]. In this section we extend the study to show a similar correlation for the coalescence of parallel line growth fronts. Two morphological categories whose cross-sectional shape was determined by mask stripe direction and growth condition were previously revealed, with V/III ratio and absolute TBP pressure being critical variables with which to tune these morphologies [9,10]. Fig. 2a–h illustrates the shape of these two categories of parallel lines grown homoepitaxially through 0.8 μm wide linear openings 60° and 30° off of [0−11]. The cross-sectional shape of growth through both categories of openings is fundamentally trapezoidal, with a set of faceted steps along either upward or downward facing sidewalls. This faceted step structure is most easily seen in Fig. 2f on the upward tilting sidewalls of the stripes oriented 30° off of [0−11]. Geometrically equivalent planes occur on the underside of the stripes oriented 60° off of [0−11] as can be seen in Fig. 2b and d. Barring extreme changes in growth conditions, the direction alone determines whether this stepped side-wall structure faces upward or downward. The proportionalities of the shapes' finer structures are readily altered via growth conditions, which most strongly affect the step size on the sidewalls. There, geometrical frustration leads to a stepped sidewall structure having low surface energy {110} facets, which if isolated define a ⟨010⟩ family stripe, combined with short "correctional" steps close to {111}A planes. The net direction of the stripe and the total proportion between the two groups of planes are interdependent. As described previously, higher V/III ratio as well as higher

absolute TBP pressures produce very sharply defined stepped sidewalls, a fact which plays strongly in the ability of neighboring stripes to coalesce [9,10].

This is critical for growths 60° off of [0−11], where coalescence initiates at the microscopically smooth upper ledge and the down-ward facing stepped sidewalls subsequently become obscured, no longer influencing the smoother morphological quality on the upper region of coalescence. The opposite is true for the growths oriented along 30° off of [0−11] having upward facing stepped sidewalls. Coalescence of these sidewalls results not only in a rough coalescent region, shown in Fig. 2g, but periodically spaced voids seen from the underside in Fig. 2h. These voids are indicative of two-zipper type coalescence and dislocation formation [13,14].

3.2. Cross-sectional and plan view TEM of coalesced homoepitaxial parallel lines

Fig. 3a shows a typical cross-sectional TEM of the coalescent region between two homoepitaxially grown lines 60° off of [0−11] by MOVPE with V/III=406. Of the three similar homoepitaxial coalescent regions examined by cross-sectional TEM, no extended defects were found. Plan view TEM of coalesced homoepitaxial lines, both 30° and 60° off of [0−11] with 5 μm separation and grown under V/III=406, was performed. A total plan view area of 140 μm² was evaluated for the 60° lines having downward facing stepped sidewalls, and was found to be without extended defects as shown in Fig. 3b. This demonstrates an upper bound of approximately 7.1×10^5 cm⁻² defects generated by coalescence of homoepitaxial parallel lines 60° off of [0−11] with 5 μm separation and 0.8 μm opening. In terms of the length of the coalesced ELO boundaries, this demonstrates an upper bound of at most 28 coalescence related defects per millimeter of coalescence. In contrast, the coalesced regions of lines 30° off of [0−11] contained a far greater number of dislocations as shown in Fig. 3c which shows a dislocation density of 1.7×10^7 cm⁻², each aligning to the angle of SAG windows.

3.3. Heteroepitaxial ELO

3.3.1. Micrometer scale mask pattern
Applying the same ELO mask of parallel lines with 0.8 μm wide openings to heteroepitaxial growth over the metamorphic buffer layer described in a previous section yielded significant morphological differences from the homoepitaxial application. As seen in Fig. 4, growth through lines of both 30° and 60° off of [0−11] extend further in the vertical [100] direction and have surfaces with increased curvature and a greater number of irregularities.
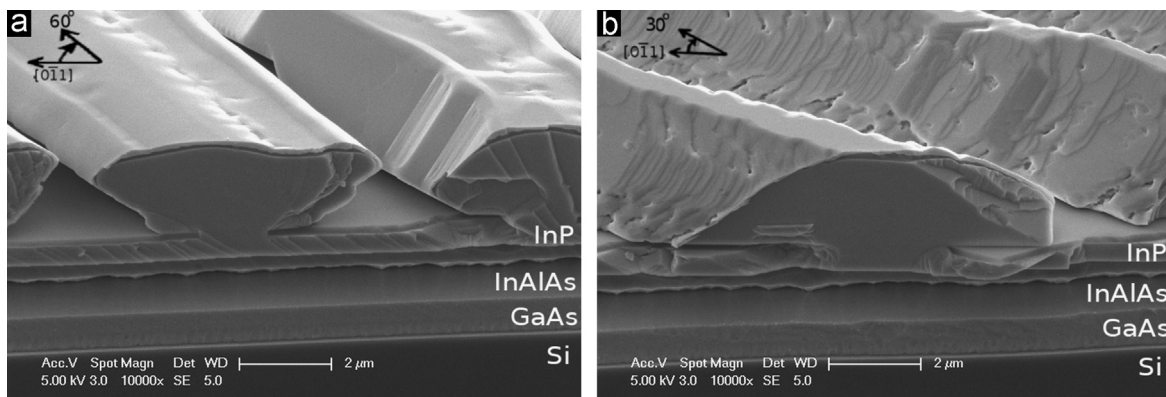

Fig. 4. Heteroepitaxial ELO growth profiles for lines oriented (a) 60° off of [0−11] and (b) 30° off of [0−11] using 0.8 μm wide openings to an InP seed layer grown on a metamorphic InAlAs layer above a GaAs buffer layer on Si. A nominal growth thickness of 1.5 μm of InP did not coalesce. The [0−11] coordinate axis and window SAG angle are drawn projected within the tilted (100) plane of the upper surface.

These variations may be attributed to the introduction of several heteroepitaxial phenomena, most notably defects and film stress at the initial SAG InP interface. Such irregular morphology is unfavorable for high quality coalesced material. To coalesce such irregular growth profiles within a reasonable film thickness, the openings must be placed significantly closer together and be made with a higher aspect ratio to terminate dislocations before reaching the laterally growing layer.

A multi quantum well (MQW) structure designed for light emission of a wavelength near 1550 nm was grown on top of the heteroepitaxial micrometer scale ELO InP for a comparison of their potential applicability to devices using non-coalesced laterally overgrown material. This MQW structure consisted of five 6.5 nm $In_{0.735}Ga_{0.265}As_{0.845}P_{0.155}$ quantum wells separated by 8 nm $In_{0.735}Ga_{0.265}As_{0.513}P_{0.487}$ barriers. Simultaneous growth upon a bare InP substrate served as a control. The resulting photoluminescence (PL) intensities seen in Fig. 5a show a clear superiority of MQW grown on lines oriented 60° off of [0−11] compared to all other investigated patterns, including lines 0°, 30°, and 90° off of [0−11], and circular "disk" openings. The differences in PL are likely due in large part to morphological effects upon quantum well uniformity and material quality, as well as the collection efficiency of the PL setup. The wider and smoother upper surface of lines 60° off of [0−11] allows for more uniform quantum well growth than the other patterns, as well as a more uniform directionality of PL emission. Varying window opening width and separation for lines 60° off of [0−11] resulted in a clear trend toward PL improvement for lines having narrower window openings (0.8 μm being the narrowest) and greater separation, as seen in Fig. 5b,c. This illustrates a correlation between laterally overgrown material area, where extended defects due to lattice mismatch are less likely to have propagated, and improved luminescence. A slight blue-shift may be attributed to adatom flux differences during selective area growth.

3.3.2. Holographically defined mask pattern

To work toward optimal coalescence of a large area film, growth through a mask of parallel lines defined holographically with a much narrower separation of 110 nm between 100 nm wide SAG openings oriented 60° off of [0−11] was explored. Such a narrow separation was chosen to encourage coalescence to initiate within a minimal thickness from the defect filtering SAG mask. As can be seen in Fig. 6a, homoepitaxial application of this pattern to a 200 nm thick SiO_2 mask layer on a (100) InP substrate yielded a microscopically smooth and continuous coalesced film after less than 1 μm of growth.

A much higher aspect ratio mask of 750 nm height, 110 nm separation, and 100 nm opening was applied to the heteroepitaxial substrate having the metamorphic buffer layer to ensure maximal dislocation filtering, as well as to explore height/opening aspect ratio upper bounds and any effect that high aspect ratios might have on planar defects. The high aspect ratio etch of SiO_2 resulted in a mask window which tapers from a 100 nm opening at the seed layer to a 180 nm opening at the upper surface, reducing lateral overgrowth to a separation of only 30 nm. From this exploration several phenomena became apparent. Among these were not only detrimental morphological effects, but also an interaction of planar defects with the SiO_2 mask.

Heteroepitaxial growth between high aspect ratio lines did not rise uniformly out of the openings, as illustrated in Fig. 6b,c. It may be noted that the initial SAG seed surface had a certain roughness, and that this may have been enhanced during the mask dry etch process and the 750 nm thick selective area growth. The presence of dislocations and other extended defects at the initial SAG surface may have also influenced the initial SAG morphology.
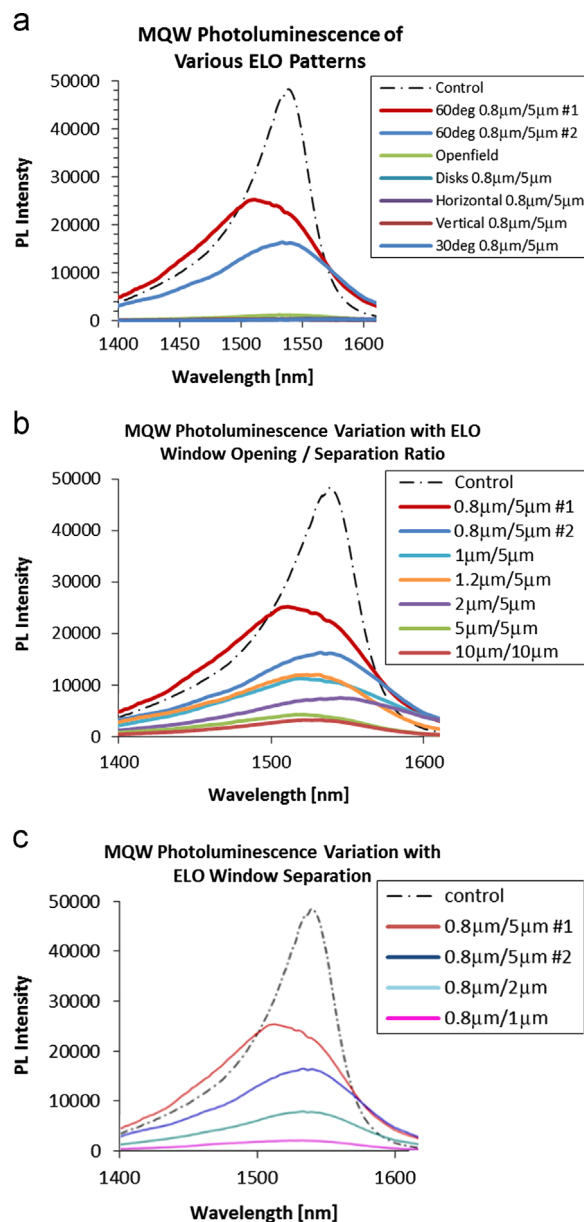

Fig. 5. (a) Photoluminescence (PL) comparison of multi quantum wells (MQW) grown using heteroepitaxial ELO from various growth mask patterns, including horizontal and vertical lines, circular disk openings, lines 30° off of [0−11], and unmasked open-field heteroepitaxy. A linear pattern oriented 60° off of [0−11] with 0.8 μm openings and 5 μm separation (denoted 0.8 μm/5 μm #1 and #2) show the greatest photoluminescence, corresponding to the growths having a semi-flat upper surface and downward facing stepped sidewalls shown in Fig. 4a. (b) and (c) show a correlation of MQW PL improvement with narrower selective area growth windows and wider separations, respectively. Each spectrum consists of one measurement with a large spot size, collecting from multiple neighboring growths. Spectra labeled 0.8 μm/5 μm #1 and 0.8 μm/5 μm #2 were taken from the same sample at different locations, demonstrating the drastic variation in PL quality that may arise from samples having non-uniform morphology and low ELO window height:width ratios.

Another factor which may have impeded uniform protrusion out of the SAG openings is the existence of a region of rough material on the upper sidewalls of the SiO_2 mask resulting from re-deposition during the ICP etch of SiO_2. As seen in Fig. 6c non-uniform growth emergence from within the SAG windows resulted in a discontinuous film.

Significant improvements in morphology were obtained by chemical mechanical polishing of the InP seed layer before ELO patterning and using a thinner (500 nm) ELO mask of holographically
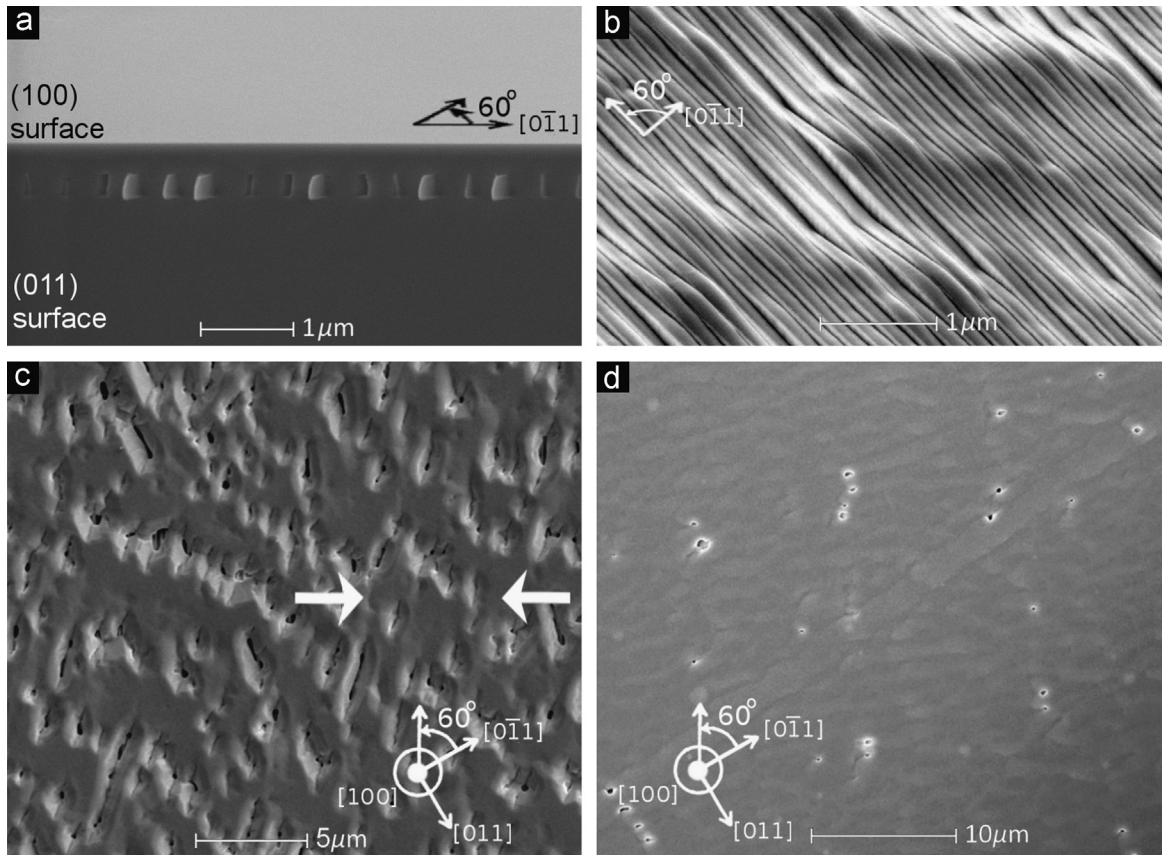
Fig. 6. Results of InP ELO grown through holographically defined lines 60° off of $[0-11]$. (a) Cleaved cross-section of a smooth and completely coalesced homoepitaxial ELO using height/width aspect ratio of 2, tilted $\sim 10°$ about $[0-11]$ to reveal the smooth coalesced surface of the upper (100) plane. Portions of the SiO_2 mask are seen protruding from the cleaved surface. (b) Heteroepitaxial growth showing non-uniform emergence and partial coalescence of InP above an ELO mask having a high aspect ratio of 7.5. The sample is tilted 60° away from [100] with an oblique perspective to best reveal the emerging growth morphology and sidewall texture. Both coordinate axes of (a) and (b) are drawn projected within the tilted (100) plane of the upper surface. (c) Plan view of a partially coalesced heteroepitaxial ELO film grown without CMP of the initial seed layer. Arrows indicate the region explored by cross-sectional TEM in Fig. 7. (d) Heteroepitaxial ELO film grown with CMP of the initial seed layer and ELO mask aspect ratio of 5.
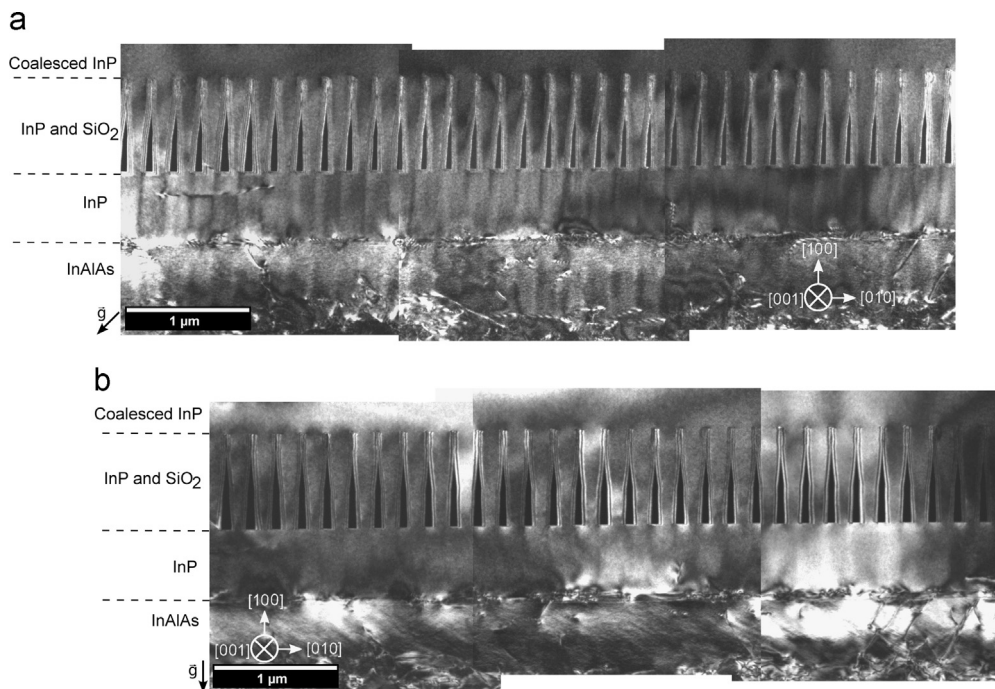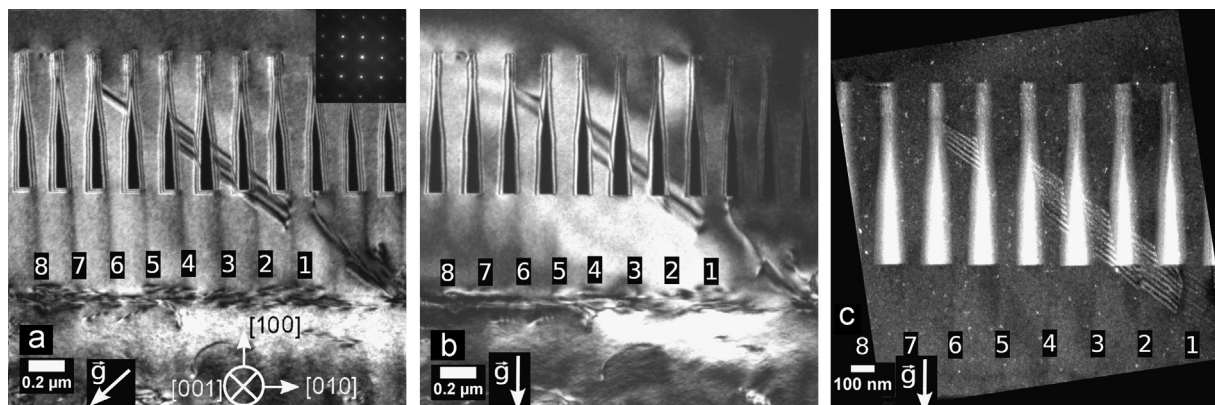

Fig. 7. Two-beam dark field cross-sectional TEM of the coalesced heteroepitaxial ELO growth region indicated in Fig. 6c. Images using two non-parallel diffraction conditions (g vectors of (a) [440], and (b) [400]) are shown to ensure that all extended defects are revealed. Lamella thinning by focused ion beam (FIB) resulted in a curtaining effect, whereby the slower milling SiO_2 caused regions of thicker InP to exist beneath the ELO mask SiO_2 than beneath the ELO window, resulting in the oscillating vertical lines of contrast within the InP seed and buffer layers in (a).

defined parallel lines. Fig. 6d shows a plan view SEM of this improved morphology resulting from a similar amount of over-growth as performed to yield Fig. 6c.

Cross-sectional TEM of a region of coalesced heteroepitaxial InP grown through high aspect ratio lines angled 60° off of [0−11]

reveals a scarcity of coalescence related dislocations. Fig. 7 shows a mosaic of a continuous region which completely lacks any dislocations in 33 consecutive points of coalescence. Fig. 8 This lamella was taken from the area identified by arrows in Fig. 6c. Those dislocations which have been observed above the ELO mask

Fig. 8. Cross-sectional TEM of a coalesced heteroepitaxial ELO film showing propagation and intermittent inhibition of a planar defect propagating through neighboring high aspect ratio SAG windows oriented 60° off of [0−11]. (a,b) Two beam dark field diffraction contrast TEM with g vectors from ⟨440⟩ and ⟨400⟩ families, respectively, showing segmented stacking fault (SF) and absence in the uppermost region. Inset of (a) shows a selective area diffraction pattern acquired through the SF seen within window 2. (c) Weak-beam dark field TEM of the same region showing a dislocation reaction with the planar defect occurring below window 1. The SF is absent from windows 5 and 7 under all three diffraction conditions. (c) was imaged using a ⟨200⟩ g vector while an ⟨800⟩ g vector was excited.
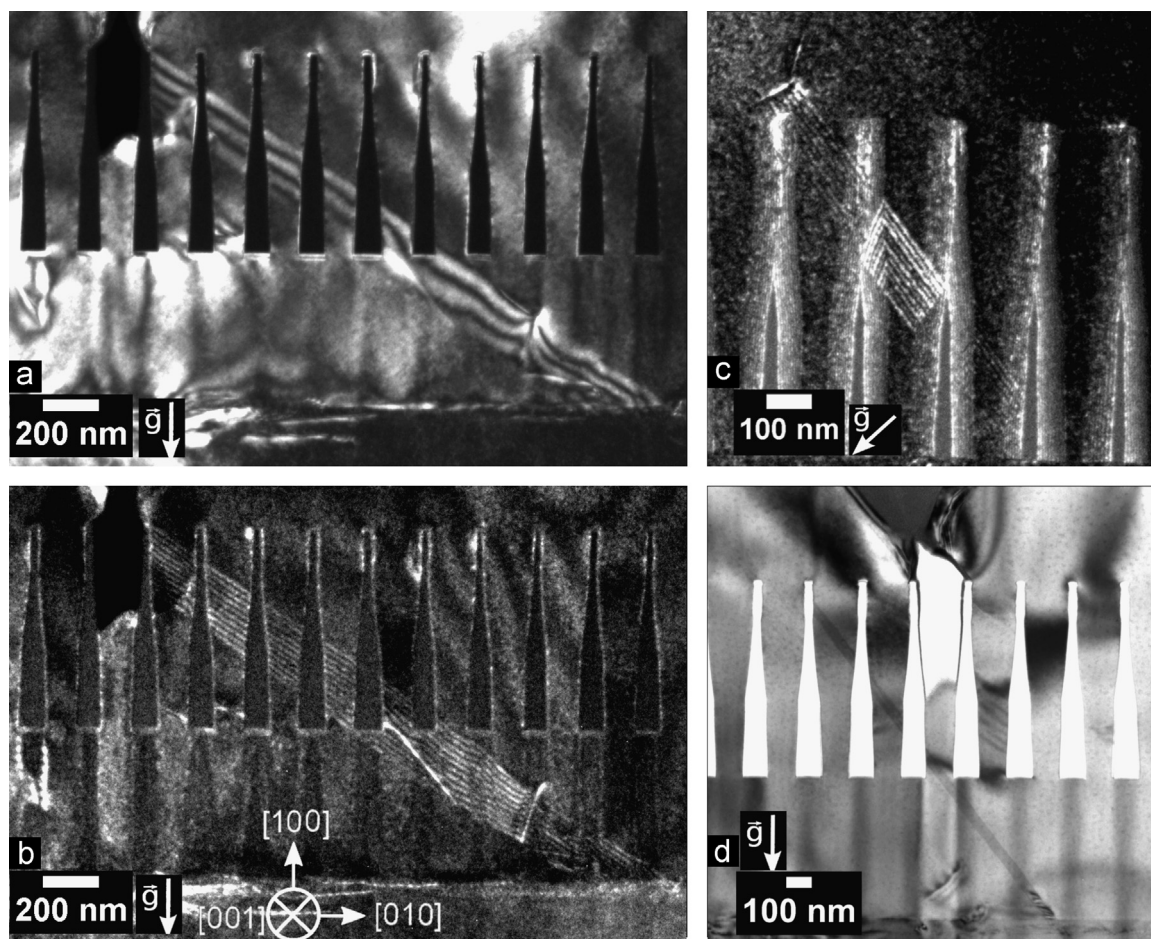
Fig. 9. Diffraction contrast TEM of ELO grown InP through lines oriented 60° off of [0−11] having an aspect ratio of 7.5, illustrating stacking fault (SF) behaviors in the presence of this mask. (a,b) Two beam dark field and weak beam dark field (WBDF) images with a ⟨400⟩ family g vector illustrating an SF contrast fringe shift in the presence of dislocations within the SF beneath the mask. (c) WBDF with a ⟨440⟩ family g vector showing SF termination upon coalescing with neighboring overgrowth above the mask, resulting in a dislocation. (d) SF which does not propagate to the ELO region above the mask. SFs in figures (c) and (d) appear with a steeper angle than the others because they exist on {111} planes rotated 90° about [100] from the SF in (a) and (b).

in other regions correlate either with termination of a stacking fault (SF), which is restricted to the small volume of material growing above the same window as the stacking fault (Fig. 9c), or are found at the coalescence of non-nearest neighbor growths which have extended over empty windows through which growth did not protrude due to morphological issues.

TEM of growth through high aspect ratio parallel lines also revealed InP stacking fault susceptibility to interactions with inhomogeneous SAG masks, a behavior which should prove useful for inhibiting their propagation into the upper layer. Fig. 8a,b shows an SF which has propagated upward from the seed layer into four neighboring windows, enumerated 1 through 8as shown. The identical periodicity of contrast fringes in these neighboring SFs, a condition met in two separate diffraction conditions, determines that they reside on parallel planes [15]. This, combined with the colinearity of the SF fringes, establishes that they are most likely coplanar and originate from the same SF within the seed layer that intersected and propagated into several neighboring SAG windows. The SF propagates upward within windows 2, 3, 4, and 6 without inhibition due to its two dimensional nature, but is absent in windows 5, 7, and the upper coalesced ELO material. Fig. 8c shows in weak-beam dark field (WBDF) contrast that the SF is not completely eliminated under window 1. A shift in the fringes beneath window 2 is indicative that either the SF experiences an additional translation along its plane, a jog to a parallel plane in that region, or that there are two partially overlapping SFs and one of them is not present where the fringe shift occurs. Additionally window 6 shows the total width of the SF decreasing and several oscillations of the contrast fringe terminating within the window. WBDF contrast did not illuminate any SF fringes in windows 5 or 7, or in the upper ELO layer. This absence along with the dislocation reaction shown occurring beneath window 1 in Fig. 8c hints at the existence of a possible means for inhibiting SF propagation, but further work is needed to elucidate the mechanisms involved.

Several more examples showing SF interaction and propagation inhibition by a high aspect ratio mask are shown in Fig. 9. In each instance examined, the SF appears to originate at the InP/InAlAs interface. Fig. 9a,b shows a similar reaction to that seen in Fig. 8, with two dislocations present within the SF beneath the mask and a shift in the fringes at the leftmost dislocation. Fig. 9a and d shows a lack of SF presence in the upper ELO layer, as well as inhibited growth occurring near an SF. The SFs in Fig. 9c and d appears to have a steeper angle because they are on {111} planes which are rotated $\pm 90°$ about [100] from those in Figs. 8 and 9a,b, thus intersecting the lamella over a shorter distance. Fig. 9c illustrates the result of an SF reaching the upper ELO coalescence boundary, wherein the SF terminates on the neighboring overgrowth and forms a dislocation at the coalesced boundary.

4. Conclusions

We have demonstrated both homoepitaxial and heteroepitaxial coalescence of InP ELO growth using MOVPE through parallel line masks. Dislocations were not seen to exist in plan-view TEM at homoepitaxial coalescent regions for parallel lines having 0.8 μm wide openings oriented 60° off of [0 – 11]. In contrast, dislocations were abundant at the coalescent regions for lines 30° off of [0 – 11] using the same growth conditions. Differences in growth morphology were emphasized as the primary difference between these two mask line directions and thus the likely cause of dislocation formation at coalescence of lines 30° off of [0 – 11]. Application of the same mask and growth conditions to heteroepitaxial ELO using a metamorphic InAlAs/GaAs buffer and InP seed layer over Si resulted in a poorer morphology, which we did

not grow to coalescence. However, photoluminescence of multi quantum wells grown on the heteroepitaxial InP emerging from lines 60° off of [0 – 11] showed a clear improvement, especially for regions with greater lateral overgrowth and narrower SAG windows. A mask of much narrower parallel lines 60° off of [0 – 11] having a larger height:opening aspect ratio of 7.50 were grown on this heteroepitaxial substrate, and cross-sectional TEM did not reveal any dislocations attributable purely to nearest neighbor coalescence. Cross-sectional TEM of these high aspect ratio parallel line ELO growths also revealed several interactions with stacking faults including an inhibition of their propagation through high aspect ratio parallel lines.

References

[1] D. Liang, A.W. Fang, H.W. Chen, M.N. Sysak, B.R. Koch, E. Lively, O. Raday, Y.H. Kuo, R. Jones, J.E. Bowers, Hybrid silicon evanescent approach to optical interconnects, Appl. Phys. A–Mater. Sci. Process. 95 (2009) 1045–1057.
[2] M. Fukuda, K. Wakita, G. Iwane, Dark defects in InGaAsP InP double heterostructure lasers under accelerated aging, J. Appl. Phys. 54 (1983) 1246–1250.
[3] S. Lourdudoss, Heteroepitaxy and selective area heteroepitaxy for silicon photonics, Curr. Opin. Solid State Mater. Sci. 16 (2012) 91–99.
[4] G. Wang, D. Nguyen, M. Leys, R. Loo, G. Brammertz, O. Richard, H. Bender, J. Dekoster, M. Meuris, M. Heyns, M. Caymax, Selective Epitaxial Growth of InP in STI Trenches on Off-Axis Si (001) Substrates 2010959–964.
[5] S. Takeuchi, K. Suzuki, Stacking fault energies of tetrahedrally coordinated crystals, Phys. Status Solidi A–Appl. Res. 171 (1999) 99–103.
[6] C. Junesand, H. Kataria, W. Metaferia, N. Julian, Z. Wang, Y.-T. Sun, J. Bowers, G. Pozina, L. Hultman, S. Lourdudoss, Study of planar defect filtering in InP grown on Si by epitaxial lateral overgrowth, Opt. Mater. Express 3 (2013) 1960–1973.
[7] G. Wang, M.R. Leys, N.D. Nguyen, R. Loo, G. Brammertz, O. Richard, H. Bender, J. Dekoster, M. Meuris, M.M. Heyns, M. Caymax, Selective Area Growth of InP in Shallow-Trench-Isolated Structures on Off-Axis Si(001) Substrates, J. Electrochem. Soc. 157 (2010) H1023–H1028.
[8] C. Merckling, N. Waldron, S. Jiang, W. Guo, O. Richard, B. Douhard, A. Moussa, D. Vanhaeren, H. Bender, N. Collaert, M. Heyns, A. Thean, M. Caymax, W. Vandervorst, Selective area growth of InP in shallow trench isolation on large scale Si(001) wafer using defect confinement technique, J. Appl. Phys. 114 (2013).
[9] N. Julian, P. Mages, C. Zhang, J. Zhang, S. Kraemer, S. Stemmer, S. Denbaars, L. Coldren, P. Petroff, J. Bowers, Coalescence of InP epitaxial lateral overgrowth by MOVPE with V/III ratio variation, J. Electron. Mater. 41 (2012) 845–852.
[10] C. Zhang, P. Mages, N. Julian, L. Coldren, S. DenBaars, J. Bowers, Growth habit control of epitaxial lateral overgrown InP by MOCVD, Opt. Soc. Am. (2011) Th17.
[11] V. Krishnamoorthy, P. Ribas, R.M. Park, Strain relief study concerning the In$_x$Ga$_{1-x}$As/GaAs (0.07 < x < 0.5) material system, Appl. Phys. Lett. 58 (1991) 2000–2002.
[12] J.I. Chyi, J.L. Shieh, J.W. Pan, R.M. Lin, Material properties of compositional graded In$_x$Ga$_{1-x}$As and In$_x$Al$_{1-x}$As epilayers grown on GaAs substrates, J. Appl. Phys. 79 (1996) 8367–8370.
[13] Z. Yan, Y. Hamaoka, S. Naritsuka, T. Nishinaga, Coalescence in microchannel epitaxy of InP, J. Cryst. Growth 212 (2000) 1–10.
[14] T. Kochiya, Y. Oyama, T. Kimura, K. Suto, J. Nishizawa, Dislocation-free large area InP ELO layers by liquid phase epitaxy, J. Cryst. Growth 281 (2005) 263–274.
[15] A. Art, R. Gevers, S. Amelinckx, The determination of the type of stacking faults in face centered cubic alloys by means of contrast effects in the electron microscope, Phys. Status Solidi B 3 (1963) 697–711.